Optimization of pump spectra for gain-flattened photonic crystal fiber Raman amplifiers operating in C-band

Kazuya Sasaki, Shailendra K. Varshney, Keisuke Wada, Kunimasa Saitoh, and Masanori Koshiba

Division of Media and Network Technologies, Hokkaido University, Sapporo 060-0814, Japan
sasaki@icp.ist.hokudai.ac.jp, skvarshney_10@yahoo.co.uk, wada@icp.ist.hokudai.ac.jp, ksaitoh@ist.hokudai.ac.jp, koshiba@ist.hokudai.ac.jp

Abstract: This paper focuses on the optimization of pump spectra to achieve low Raman gain ripples over C-band in ultra-low loss photonic crystal fiber (PCF) and dispersion compensating PCFs (DCPCFs). Genetic algorithm (GA), a multivariate stochastic optimization algorithm, is applied to optimize the pump powers and the wavelengths for the aforesaid fiber designs. In addition, the GA integrated with full-vectorial finite element method with curvilinear edge/nodal elements is used to optimize the structural parameters of DCPCF. The optimized DCPCF provides broadband dispersion compensation over C-band with low negative dispersion coefficient of −530 ps/nm/km at 1550 nm, which is five times larger than the conventional dispersion compensating fibers with nearly equal effective mode area (21.7 μm^2). A peak gain of 8.4 dB with ±0.21 dB gain ripple is achieved for a 2.73 km long DCPCF module when three optimized pumps are used in the backward direction. The lowest gain ripple of ±0.36 dB is attained for a 10 km long ultra-low loss PCF with three backward pumps. Sensitivity analysis has been performed and it is found that within the experimental fabrication tolerances of ±2%, the absolute magnitude of dispersion may vary by ±16%, while the Raman gain may change by ±7%. Through tolerance study, it is examined that the ring core's hole-size is more sensitive to the structural deformations.

OCIS codes: (060.2280) Fiber design and fabrication; (060.2400) Fiber properties.

References and links

1. C. Headly and G. P. Agarwal, *Raman Amplification in Fiber Optical Communication Systems*, (Academic Press, New York, 2004).
2. M. N. Islam, *Raman Amplification for Telecommunications 1*, (Springer, 2003).
3. Y. Emori, Y. Akasaka, and S. Namiki, "Broadband lossless DCF using Raman amplification pumped by multichannel WDM laser diodes," Electron. Lett. **34**, 2145-2146 (1998).
4. M. Achtenhagen, T. G. Chang, and B. Nyman, "Analysis of a multiple-pump Raman amplifier," Appl. Phys. Lett. **78**, 1322-1324 (2001).
5. V. E. Perlin and H. G. Winful, "Optimal design of flat-gain wide-band fiber Raman amplifiers," J. Lightwave Technol. **20**, 250-254 (2002).
6. S. Cui, J. Liu and X. Ma, "A novel efficient optimal design method for gain-flattened multiwavelength pumped fiber Raman amplifier," IEEE Photon. Technol. Lett. **16**, 2451-2453 (2004).
7. K. Thyagarajan and C. Kakkar, "Novel fiber design for flat gain Raman amplification using single pump and dispersion compensation in S band," J. Lightwave Technol. **22**, 2279-2286 (2004).
8. T. J. Ellingham, L. M. Gleeson, and N. J. Doran, "Enhanced Raman amplifier performance using nonlinear pump broadening," in *proceedings of IEEE European Conference on Optical Communication* (IEEE, 2002), pp. 1-2.
9. T. J. Ellingham, J. D. Ania-Castanin, S. K. Turitsyn, A. Pustovskikh, S. Kobtesev, and M. P Fedoruk, "Dual pump Raman amplification with increased flatness using modulation instability," Opt. Express **13**, 1079-1084 (2005).

#78520 - $15.00 USD Received 2 January 2007; revised 31 January 2007; accepted 20 February 2007

10. S. Martin Lopez, M. Gonzalez-Herralez, P. Corredera, M. L. Hernanz, and A. Carrasco, "Gain-flattening of fiber Raman amplifiers using non-linear pump spectral broadening," Opt. Commun. **242**, 463-469 (2004).
11. T. A. Birks, J. C. Knight, and P. St. J. Russell, "Endlessly single-mode photonic crystal fiber," Opt. Lett. **22**, 961-963 (1997).
12. N. A. Moretensen, M. D. Nielsen, J. R. Folkenberg, A. Petersson, and H. R. Simonsen, "Improved large mode area endlessly single mode photonic crystal fibers," Opt. Lett. **28**, 393-395 (2003).
13. A. Bjarklev, J. Broeng, and A. S. Bjarklev, *Photonic Crystal Fibres*, (Kulwer Academic Publishers 2003).
14. K. Saitoh and M. Koshiba, "Chromatic dispersion control in photonic crystal fibers: Application to ultra-flattened dispersion," Opt. Express **11**, 843-852 (2003).
15. T. M. Monro, D. J. Richardson, N. G. R. Broderick, and P. J. Bennett, "Holey optical fibers: an efficient modal model," J. Lightwave Technol. **17**, 1093-1102 (1999).
16. R. K. Sinha and S. K. Varshney, "Dispersion properties of photonic crystal fibers," Microwave Opt. Technol. Lett. **37**, 129-132 (2003).
17. F. Gérome, J. L. Auguste, and J. M. Blondy, "Design of dispersion-compensating fibers based on a dual-concentric-core photonic crystal fiber," Opt. Lett. **29**, 2725-2727 (2004).
18. M. Fuochi, F. Poli, A. Cucinotta, and L. Vincetti, "Study of Raman amplification properties in triangular photonic crystal fibers," J. Lightwave Technol. **21**, 2247-2254 (2003).
19. M. Bottacini, F. Poli, A. Cucinotta, and S. Selleri, "Modeling of photonic crystal fiber Raman amplifiers," J. Lightwave Technol. **22**, 1707-1713 (2004).
20. Z. Yusoff, J. H. Lee, W. Belardi, T. M. Monro, P. C. Teh, and D. J. Richardson, "Raman effects in a highly nonlinear holey fiber: amplification and modulation," Opt. Lett. **27**, 424-426 (2002).
21. C. J. S. de Matos, K. P. Hansen, and J. R. Taylor, "Experimental characterization of Raman gain efficiency of holey fiber," Electron. Lett. **39**, 424-425 (2003).
22. S. K. Varshney, K. Saitoh, and M. Koshiba, "A novel fiber design for dispersion compensating photonic crystal fiber Raman amplifier," IEEE Photon. Technol. Lett. **17**, 2062-2065 (2005).
23. S. K. Varshney, T. Fujisawa, K. Saitoh, and M. Koshiba, "Novel design of inherently gain-flattened discrete highly nonlinear photonic crystal fiber Raman amplifier and dispersion compensation using a single pump in C-band," Opt. Express **13**, 9516-9526 (2005).
24. S. K. Varshney, T. Fujisawa, K. Saitoh, and M. Koshiba, "Design and analysis of a broadband dispersion compensating photonic crystal fiber Raman amplifier operating in S-band," Opt. Express **14**, 3528-3540, (2006).
25. F. Poli, L. Rosa, M. Bottacini, M. Foroni, A. Cucinotta, and S. Selleri, "Multipump flattened-gain Raman amplifiers based on photonic crystal fibers," IEEE Photon. Technol. Lett. **17**, 2556-2558 (2005).
26. The GA toolbox, MATLAB 7.0, www.mathworks.com
27. K. Tajima J. Zhou, K. Nakajima, and K. Sato, "Ultralow loss and long length photonic crystal fiber," J. Lightwave Technol. **22**, 7-10 (2004).
28. K. Saitoh and M. Koshiba, "Full-vectorial imaginary-distance beam propagation method based on a finite element scheme: application to photonic crystal fibers," IEEE J. Quantum Electron. **38**, 927-933 (2002).
29. T. Fujisawa, K. Saitoh, K. Wada, and M. Koshiba, "Chromatic dispersion profile optimization of dual-concentric-core photonic crystal fibers for broadband dispersion compensation," Opt. Express **14**, 893-900 (2006).
30. L.G. Nielsen, M. Wandel, P. Kristensen, C. Jorgensen, L. V. Jorgensen, B. Edvold, B. Palsdottir, and D. Jakobsen, "Dispersion compensating fibers," J. Lightwave Technol. **23**, 3566-3579 (2005).
31. J. Bromage, K. Rottwitt, and M. E. Lines, "A method to predict the Raman gain spectra of germanosilicate fibers with arbitrary index profiles," IEEE Photon. Technol. Lett. **14**, 24-26 (2002).
32. Z. Michalewicz, *Genetic Algorithms + Data Structures = Evolution Programs*, (Springer-Verlag, New York, 1992).
33. X. Liu and Y. Li, "Efficient algorithm and optimization for broadband Raman amplifiers," Opt. Express **12**, 564-573 (2004).
34. The numerical data of Raman gain efficiency for conventional dispersion compensating fibers was provided by Furukawa Elect. Co. (Ltd.).
35. http://www.ofs.dk/DCRA_note_0103.pdf
36. S. G. Leon-Saval, T. A. Birks, N. Y. Joy, A. K. George, W. J. Wadsworth, G. Kakarantzas, and P. St. J. Russell, "Splice-free interfacing of photonic crystal fibers," Opt. Lett. **30**, 1629-1634 (2005).
37. P. J. Roberts, B. J. Mangan, H. Sabert, F. Couny, T. A. Birks, J. C. Knight, and P. St. J. Russell, "Control of dispersion in photonic crystal fibers," J. Opt. Fiber. Commun. Rep. **2**, 435-461 (2005).

1. Introduction

Fiber Raman amplifiers (FRAs) have emerged as elegant solutions to enhance the bandwidth of wavelength division multiplexed (WDM) and dense WDM transmission networks due to (1) their ability to operate in any band of transmission networks prior to the availability of a suitable pump and (2) the reduction of the noise figure. Typically, FRAs based on stimulated Raman scattering process consist of a gain medium (i.e. optical fiber) and a pump or multi-pumps either placed in co- or contra-direction. FRAs can be distinguished in two categories, namely distributed FRA where the gain is distributed along the length of the fiber and discrete

#78520 - $15.00 USD Received 2 January 2007; revised 31 January 2007; accepted 20 February 2007

or lumped FRA where dispersion compensating fibers (DCFs) are the gain medium [1, 2]. For the practical use of FRAs in optical telecom links, the gain flatness is one of the important issues to provide an equal amount of gain to every signal. To resolve this problem, several pumps [3-6] in both co- and counter propagation schemes have been employed to achieve the lowest gain ripples in conventional FRAs. However, gain ripples can also be lowered either by modifying fiber designs [7] and using a single pump with added dispersion compensation functionality or by using a nonlinear spectral pump broadening [8-10].

In recent years, photonic crystal fibers (PCFs), special kind of optical fibers, where micro-sized air-channels run along the propagation direction, have boosted optical fiber technology due to their superior optical properties over conventional optical fibers such as, ultra-wide band single mode operation [11], small or large [12] effective mode area, and overall manageable dispersion properties [13-17]. The small effective mode area in PCFs results due to large degrees of freedom in geometrical parameters, which can gives rise to high nonlinearity and thus high Raman gain efficiency (RGE) that is defined as the Raman gain coefficient per unit effective mode area [18]. This suggests PCFs to act as a strong Raman gain medium. In past, Raman amplification properties of PCFs have been studied theoretically [19] where a model was proposed to obtain Raman performances of a low-loss PCF. Yusoff *et al*. [20] have experimentally obtained Raman gain in U-band in a highly nonlinear holey fiber, while Matos *et al*. [21] have measured the RGE of a PCF. Recently, authors have also proposed PCFs based Raman amplifier modules [22-24] which incorporate two key functionalities, namely, Raman amplification and dispersion compensation into a single component. The fiber designs were tailored to achieve the gain-flattened Raman characteristics in S- and C wavelength bands by using a single pump. So far, the lowest gain ripples (GRs) in PCF Raman amplifiers were accomplished through modification in fiber designs, but no proper optimization technique has been applied to find the optimal pump profile to achieve the best gain flatness. Recently, an effort has been made by Poli *et al.* [25] to obtain the gain flattened PCF Raman amplifier at the expense of five pumps using a superposition method.

In this paper, we optimize the pump spectra (wavelengths and powers) by using a genetic algorithm (GA) [26] to achieve low GR in PCF-based Raman amplifiers. Three different examples of PCFs have been considered; ultra-low loss PCF [27] (ULL-PCF) and dispersion compensating PCFs (DCPCFs). To the best of author's knowledge, optimization of pump spectra based on GA will be applied to PCF-based amplifiers for the first time. Further, a full vectorial finite element method (V-FEM) combined with GA is used to accurately determine the DCPCF structural parameters [28, 29]. The V-FEM with curvilinear edge/nodal elements is used to precisely calculate the dispersion characteristics of ULL-PCF and DCPCFs. The optimized DCPCF provides a broadband dispersion compensation over C-band with the largest negative dispersion of −530 ps/nm/km and effective mode area of 21.7 μm^2 at 1550 nm wavelength. The module comprised of a 2.73 km long DCPCF can compensate the positive dispersion accumulated over an 80 km long conventional single mode fiber (SMF) link with a residual dispersion below ±0.47 ps/nm/km in C-band. It has been found that three pumps operating in the backward direction of a 10 km long ultra-low loss PCF provide a peak gain of 8.8 dB with ±0.36 dB GR, while a maximum gain of 8.4 dB with ±0.21 dB of GR is attained in a 2.73 km module of DCPCF over C-band.

This paper is organized as follows. In section 2, we have described the fiber geometries, the procedure for determining the optimized structural parameters of DCPCF, and the basic modal characteristics of PCFs. The Raman amplification model is briefly described in section 3 where the RGE and Rayleigh backscattering coefficient of PCFs are evaluated. Then, in section 4, we have discussed the optimization of pump spectra for both ULL-PCF and the optimized DCPCF structures. Raman characteristics such as optical signal to noise ratio (OSNR), noise figure (NF), and double Rayleigh backscattering (DRB) have been obtained for optimized pump profile of the corresponding fiber designs. The feasibility and the sensitivity of the fiber tolerances are discussed in section 5 while the summary of the work is included in section 6.

#78520 - $15.00 USD Received 2 January 2007; revised 31 January 2007; accepted 20 February 2007

2. Fiber design and optimization

This section describes the fiber designs, the optimization method to find the optimum DCPCF structural parameters, and their modal properties. Figures 1(a), 1(b), and 1(c) show the transverse cross-section of ULL-PCF and DCPCFs, where the air-holes are arranged in a triangular lattice with an uniform lattice constant Λ. The ULL-PCF that was fabricated up to 10 km in length exhibits the lowest attenuation of 0.37 dB/km at 1550 nm [27]. The fabricated ULL-PCF has a pitch constant of 4.0 μm and hole-diameter of 2.5 μm. The fiber shows an effective mode area of 16.4 μm^2 at 1550 nm.

We have considered two different designs of DCPCFs for present analysis. The first design, whose design parameters were manually obtained and the dispersion and Raman characteristics were published in Ref. [22], will be referred as type-1 DCPCF, while the second DCPCF design whose structural parameters are optimized by GA will be named hereafter as type-2 DCPCF. To achieve a large negative dispersion over C-band, dual concentric core approach is used for designing DCPCFs. In type-1 design, the ring core was created at 2nd air-hole ring, while in type-2, the ring-core was built from 2nd to 7th air-hole ring with a reduced hole-diameter of d_s as shown in Figs. 1(b) and 1(c). The air-holes surrounding the central core and in the outermost hole rings have hole diameter d, such that $d>d_s$. The opto-geometrical parameters d, d_s, and Λ are well optimized by GA algorithm as discussed in Ref. [29]. The following fitness function F (Λ, d/Λ, d_s/Λ) was considered to obtain an optimal value of d, d_s, and Λ such that type-2 DCPCF exhibits a slowly varying negative dispersion and can compensates for dispersion slope.

$$F\left(\Lambda, \frac{d}{\Lambda}, \frac{d_s}{\Lambda}\right) = \exp\left(w_1 f_1 + f_2\right) \tag{1}$$

with

$$f_1 = -\sum_{\lambda=1.53\mu m}^{\lambda=1.565\mu m} \left| D_{\text{target}}(\lambda) + D_{\text{DCPCF}}(\lambda) \right| \tag{2}$$

$$f_2 = \begin{cases} -0.9\exp(w_1 f_1) & \text{if} \quad A_{eff}\,@1.55\,\mu\text{m} < 20\,\mu\text{m}^2 \\ 0 & \text{else} \end{cases} \tag{3}$$

where w_1 is a scaling parameter and taken as 0.001, A_{eff} is the effective mode area, D_{DCPCF} is the dispersion coefficient of DCPCF, and λ is the free space wavelength. D_{target} is defined as

$$D_{\text{target}}(\lambda) = X \times D_{\text{SMF}} \tag{4}$$

where X is the integer and D_{SMF} is the dispersion coefficient of SMF. f_1 corresponds to the dispersion slope compensation and if D_{SMF} is completely compensated by DCPCF f_1 is zero and F becomes to its maximum value of 1. f_2 is the penalty term with regard to A_{eff}, and the structure having smaller effective area will be discarded in GA analysis. The constraint on effective mode area was applied to ensure that DCPCF should have a similar effective mode area as of conventional DCF and the mode-field should nearly match to the mode-field of conventional SMF so that splice loss between two can be decreased and nonlinearity can be reduced. On the basis of GA, the optimized structural parameters for type-2 DCPCF are obtained as d = 0.955 μm, d_s = 0.706 μm, and Λ= 1.81 μm.

#78520 - $15.00 USD Received 2 January 2007; revised 31 January 2007; accepted 20 February 2007

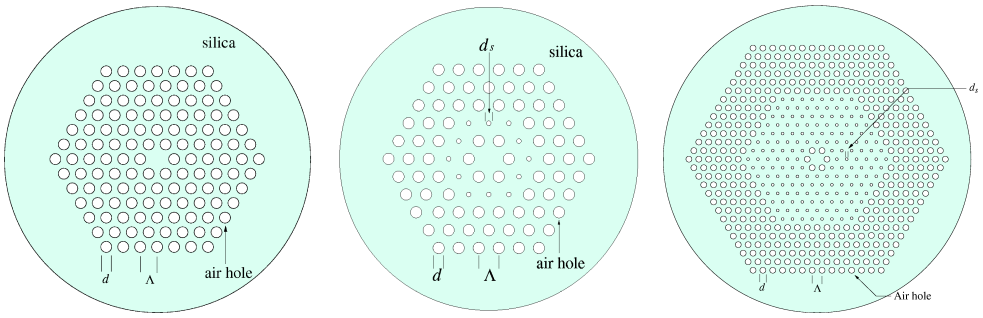

(a) (b) (c)

Fig. 1. Transverse cross-section of (a) ULL-PCF (d/Λ=0.625 and Λ=4.0 μm) [27] (b) type-1 DCPCF (d/Λ=0.7, d_s/Λ=0.26, and Λ=2 μm) [22], and (c) type-2 DCPCF (d/Λ=0.527, d_s/Λ=0.39, and Λ=1.81μm) optimized through GA. The background material is silica while circles represent the air-holes.

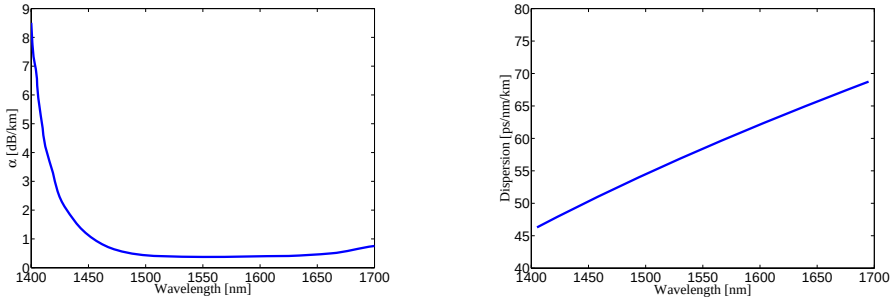

(a) (b)

Fig. 2. (a). Attenuation spectrum and (b). dispersion characteristics of ULL-PCF [25]. The ULL-PCF shows a loss of 0.37 dB/km at 1550 nm and exhibits anomalous dispersion characteristics.

Table 1. Fiber's parameters and their modal properties.

Fiber property	ULL-PCF	Type-1 DCPCF	Type-2 DCPCF
Λ [μm]	4.0	2.0	1.89
A_{eff}[μm^2] @ 1550 nm	16.4	11.3	21.7
D [ps/nm/km] @1550 nm	58.4	−240	−530

Figures 2(a) and 2(b) depict the attenuation and dispersion spectrum of ULL-PCF. The fiber shows an attenuation of 0.37 dB/km at 1550 nm and exhibits anomalous dispersion over wavelength range of interest. Figure 3(a) represents the dispersion characteristics of type-1 (solid blue curve) and type-2 (solid red curve) DCPCFs. The material dispersion of silica has been taken into account by three-term Sellemier's formula. Due to small pitch of type-2 DCPCF, fiber shows large negative dispersion in comparison to type-1 DCPCF. The dispersion exhibited by both DCPCFs at 1550 nm is –240 ps/nm/km and –530 ps/nm/km, respectively. Since both DCPCFs show different dispersion coefficients and hence the length required for the compensation of the dispersion accumulated in a pool (80 km) of SMF link

#78520 - $15.00 USD Received 2 January 2007; revised 31 January 2007; accepted 20 February 2007

will be different. By a standard mathematical relationship [30] between the length of DCF and dispersion coefficient of the compensating fiber, the length of type-1 and type-2 DCPCFs are calculated, respectively, as 5.2 km and 2.73 km. The variation of link residual dispersion over C-band is depicted in Fig. 3(b) for both DCPCFs. It can be clearly seen that the link residual dispersion stays below ±0.47 ps/nm/km over C-band. Note that the dispersion coefficient of type-2 DCPCF is five times larger than the conventional DCF [30] with nearly equal effective mode area (21.7 μm^2). Table 1 summarizes the fiber's parameters and their important modal characteristics.

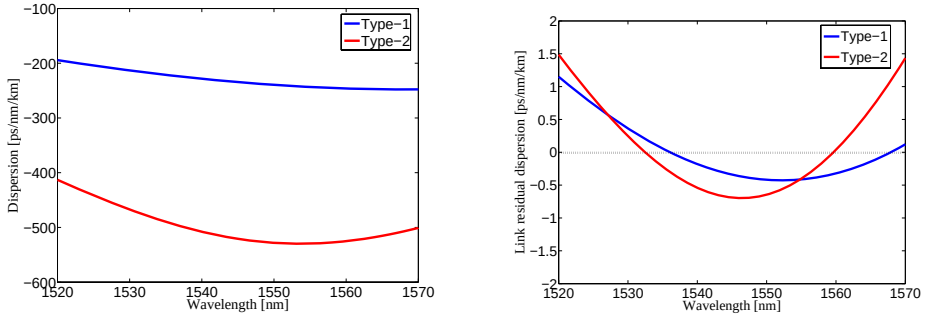

(a) (b)

Fig. 3. (a). Dispersion characteristics and (b). the spectral variation of link residual dispersion for type-1 DCPCF (solid blue curve) and type-2 DCPCF (solid red curve). The type-1 and type-2 DCPCFs exhibit dispersion of −240 ps/nm/km and −530 ps/nm/km, respectively, at 1550 nm.

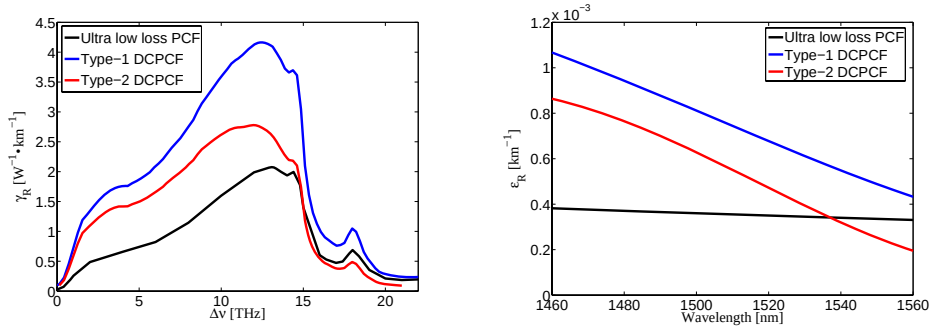

(a) (b)

Fig. 4. (a). RGE as a function of frequency shift and (b). Rayleigh backscattering coefficient as a function of the wavelength for ULL-PCF, type-1, and type-2 DCPCFs. The peak RGE (2.1 $W^{-1}.km^{-1}$) is obtained at 13.1 THz for ULL-PCF, while the peak RGE of 4.17 $W^{-1}.km^{-1}$ and 2.8 $W^{-1}.km^{-1}$ occur at 13.0 THz for type-1 and type-2 DCPCFs, respectively, for a depolarized pump of 1455 nm wavelength.

3. Raman amplification model for PCFs

In this section, we describe a model to obtain Raman amplification characteristics of ULL-PCF and DCPCFs. The RGE, one of the important parameter's required to solve propagation equations, is computed as [18, 23, 31]

$$\gamma_R = \iint_S C_{\mathrm{SiSi}}(\Delta\nu)\; i_{\mathrm{s}}(x,y)\; i_{\mathrm{p}}(x,y)\; dx\; dy \tag{5}$$

where i_s and i_p are the normalized signal and pump intensities obtained through an exact definition of Poynting vector [18] which is calculated by V-FEM. S is the PCF cross-section, and $C_{\mathrm{SiSi}}(\Delta\nu)$ is the Raman gain spectra of Si-O-Si bounds [31] for a depolarized pump of

#78520 - $15.00 USD Received 2 January 2007; revised 31 January 2007; accepted 20 February 2007

1455 nm. The RGE spectrum as a function of the frequency shift (Δν) for ULL-PCF (solid black curve), type-1 (solid blue curve) and type-2 (solid red curve) DCPCFs is plotted in Fig. 4(a), while the spectral variation of Rayleigh backscattering coefficient (ε_R) for corresponding fiber designs has been illustrated in Fig. 4(b). The Rayleigh backscattering coefficient for PCFs is calculated [19, 23] as

$$\varepsilon_R(\lambda) = \frac{3}{8\pi\lambda^2 n_{\mathrm{Si}}^2} \iint_S C_R \; i^2(x,y) \; dx \; dy \,, \tag{6}$$

where n_{Si} is the refractive index of silica, C_R is the Rayleigh scattering coefficient which is assumed to be 1 dB/km/μm^4, $i(x, y)$ is the normalized field intensity of a signal, and λ is the desired wavelength.

The RGE spectrum reveals two peaks around its maximum for ULL-PCF which is due to Raman nature of silica glass. The ULL-PCF shows a peak of 2.1 W^{-1}.km^{-1} around a frequency shift of 13.1 THz, while type-1 and type-2 DCPCFs show the single peak of 4.17 W^{-1}.km^{-1} and 2.8 W^{-1}.km^{-1} around a frequency shift of 13 THz. Note that type-1 DCPCF shows higher RGE which is due to its small effective mode area that allows a strong overlap between pump and signal field intensities before the phase matching wavelength (PMW) between the individual core modes. From Fig. 4(b) it can be clearly seen that type-1 DCPCF has larger Rayleigh backscattering coefficient than the type-2 DCPCF, and ULL-PCF.

4. Optimization of pump spectra

The selection of the pump wavelengths and powers by a trial and error approach is a tedious way to design a FRA with flat Raman gain characteristics. Therefore, we employ an optimization technique which is based on the GA to optimize the pump spectra namely the initial pump power and wavelength to attain minimum GR. The GA, a multivariate stochastic optimization algorithm, based on natural selection and natural genetics, is generally able to find more accurate solutions in a reasonable amount of time [32] and has been used by many researchers [6, 33] to optimize pump spectra in order to achieve flat gain in conventional optical FRAs. The GA repeatedly modifies a population of individual solutions. At each step the GA selects individuals at random from the current population to be parents and uses them to produce the children for next generation. Over successive generation, the population "evolves" toward an optimal solution. The use of GA requires the determination of the chromosome representation, the creation of initial population, the determination of the fitness function, the selection of function, and the termination criteria [32].

For any GA, an "individual" i.e. number of variables is a feasible solution which is described by "chromosome". At the first generation, a population of "individuals" (pump wavelengths and powers) is randomly created. After generating an initial population (which is 20 in our case) that contains a certain number of individuals, a series of processes (selection, crossover, and mutation) is performed on the population to produce the next generation. The GA keeps on running from generation to generation by selecting and reproducing parents until a termination criterion is satisfied. The most frequently used stopping criterion is a specified number of generations, which we have defined as 50, a number that is sufficient to obtain optimal solution. The following fitness function $F(\lambda_k, P_k)$ is defined to achieve the optimal solutions,

$$F(\lambda_k, P_k) = \begin{cases} \dfrac{G_{\max}(\lambda_k, P_k) - G_{\min}(\lambda_k, P_k)}{2} & \text{if} \quad G_{\max} > 8 \text{ [dB]} \\ 1000 & \text{else} \end{cases} \tag{7}$$

with

#78520 - $15.00 USD Received 2 January 2007; revised 31 January 2007; accepted 20 February 2007

$$G = 10\log_{10}\frac{P_S^+(L)}{P_S(0)} \tag{8}$$

where λ_k and P_k are the pump wavelengths and pump powers, and k = 1, 2 m with m as number of pumps used, L denotes the length of the fiber, G is the Raman gain and defined by (8). The optimization problem is solved in MATLAB using its GA toolbox [26] on a 3.2 GHz windows based PC. It took nearly 48-72 hours to find the optimal pump profiles for different fiber designs. In our optimization procedure, we have defined a fitness function (7)-(8) that governs the gain ripples accurately and used a constraint to yield moderate gain values using GA toolbox of MATLAB.

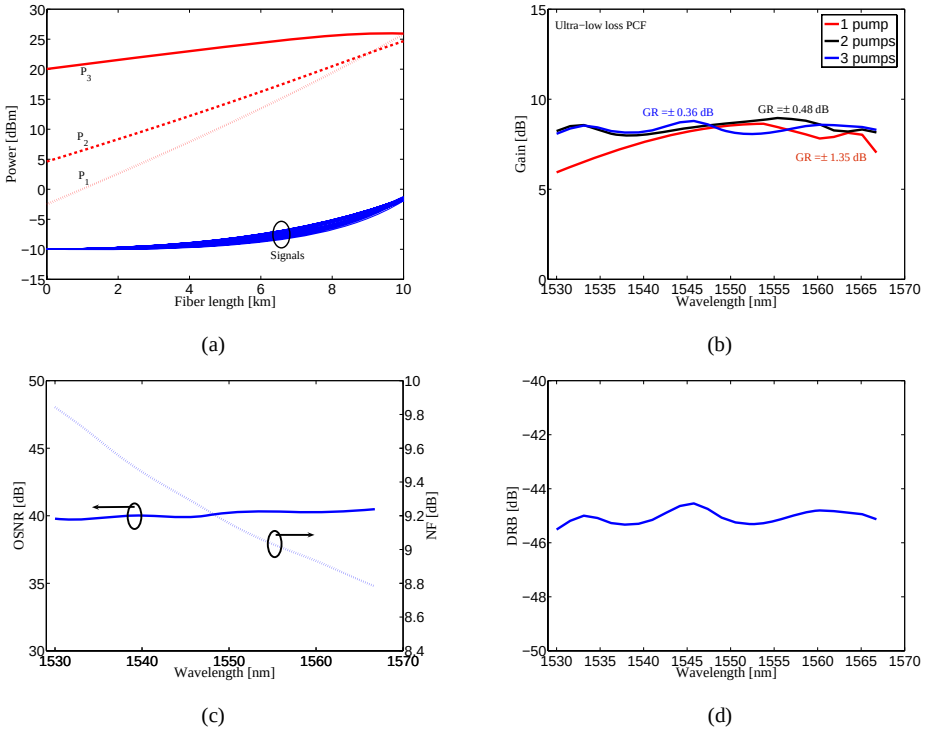

Fig. 5. (a). Power evolution of pumps and signals along the distance of fiber and the spectral variation of (b). gain, (c). OSNR, NF, and (d). DRB of a 10 km long ultra-low loss PCF. It can be clearly seen that with three pumps, the fiber shows the lowest GR of ±0.36 dB with a peak gain of 8.8 dB over C-band.

Table 2. Optimized pump powers and wavelengths for 10 km long ULL-PCF.

m	λ_1 [nm]	λ_2 [nm]	λ_3 [nm]	P_1 [mW]	P_2 [mW]	P_3 [mW]	Total power [mW]	GR [dB]	Max gain [dB]	OSNR ripple [dB]
1	1454.5			720			720	±1.35	8.6	±0.43
2	1425.6	1456.0		483	570		1053	±0.48	8.9	±0.42
3	1426.2	1436.9	1465.6	383	293	392	1068	±0.36	8.8	±0.38

#78520 - $15.00 USD Received 2 January 2007; revised 31 January 2007; accepted 20 February 2007

4.1 Gain characteristics of ultra-low loss PCF

We have fixed the following set of parameters in our simulations; three pumps travel in the backward direction and twenty four signal channels spaced at 200 GHz from 191.27 THz to 196.08 THz with an input power of −10 dBm/ch in the forward direction. The backward reflections of the signals from the fiber end, the amplified spontaneous emission, and the single Rayleigh backscattering in both forward and backward directions have been considered in model as mentioned in Ref. [23]. On the basis of GA, the power evolution of three pumps and twenty four signals along fiber length is depicted in Fig. 5(a). The dotted, dashed, and solid red curves correspond to pumps 1, 2, and 3, respectively, while the solid blue curves stand for the signals. The spectral variation of the gain attained by the signals in a 10 km long ULL-PCF for different set of pumps is exhibited in Fig. 5(b). When a single pump is used (solid red curve), an 8.6 dB of maximum gain can be achieved with ±1.35 dB GR, while the GR decreases to ±0.48 dB by using two pumps (solid black curve). Further, by increasing the number of pumps to three, we found that the GR can be reduced to ±0.36 dB with a peak gain of 8.8 dB. The corresponding gain curve is shown by solid blue curve in Fig. 5(b). A total pump power of 1068 mW was used to achieve the lowest GR in ULL-PCF based Raman amplifier.

On the basis of the optimized pump spectra and signal values, the corresponding OSNR, DRB, and NF are calculated from the formulae described in Ref. [23]. The variation of OSNR (solid blue curve), NF (dotted blue curve), and DRB (solid blue curve) for the optimized pump profile are illustrated in Figs. 5(c) and 5(d), respectively. It is evident from the figures that a high OSNR (>35dB) with ±0.38 dB ripple, low DRB values, and low NF (<9.8 dB) with an offset of 0.9 dB can be achieved in a 10 km long ULL-PCF Raman amplifier. In a comparison to Ref. [25], where a superposition method was employed to achieve the almost similar GR in ULL-PCF with five numbers of pumps, we have succeeded to reduce the number of pumps by applying a more accurate optimization procedure. The pump powers with corresponding wavelengths, GR, peak gain and OSNR ripples are tabulated in Table 2 for a 10 km long ULL-PCF Raman amplifier, where the index *m* tells about the number of pumps.

4.2 Gain characteristics of type-1 DCPCF

In this subsection, we study the Raman performance of type-1 DCPCF. The power evolutions of pumps and signals are shown in Fig. 6(a). The dotted, dashed, and solid red curves correspond to pumps 1, 2, and 3, respectively, while the solid blue curves stand for the signals. Due to the lack of experimental measurement of attenuation spectrum for DCPCFs with dual concentric cores, we have considered an attenuation spectrum of an ultra-low loss regular PCF [27] and raised the attenuation coefficient to 0.58 dB/km at 1550 nm. The attenuation value of 0.58 dB/km is almost near to the attenuation of a high delta conventional optical fiber

From Table 3 and Fig. 6(b), we can deduce that the GR are ± 1.2 dB (one pump, solid red curve), ±0.8 dB (two pumps, solid black curve), and ±0.4 dB (three pumps, solid blue curve); the total input powers of the individual set of pumps are 520 mW, 770 mW, and 690 mW, respectively. A peak gain of 21.6 dB is achieved in a 5.2 km long type-1 DCPCF Raman amplifier. Further, to compare with existing DCF Raman gain performances whose RGE data was provided by Furukawa Elec. Co. Ltd. [34], we have considered similar pump power, wavelength, fiber length and attenuation spectrum as of DCPCF and found ±2.9 dB of GR (solid green curve) in conventional DCF Raman amplifier by using a single pump. Note that the conventional DCF shows a dispersion of approximately −120 ps/nm/km at 1550 nm. This comparison between DCPCF Raman amplifier and conventional DCF Raman amplifier proves the superiority of PCFs over conventional ones. Figures 6(c) and 6(d) present the spectral variation of OSNR, NF, and DRB in a 5.2 km long type-1 DCPCF Raman amplifier. The module shows high OSNR (>27 dB), low NF (<9 dB), and relatively high DRB values. It is worthy to mention that the zero dispersion wavelength of the fiber is 1421.46 nm which expels the possibility of generating the dominant nonlinear effects such as four-wave mixing.

#78520 - $15.00 USD Received 2 January 2007; revised 31 January 2007; accepted 20 February 2007

4.3 Gain characteristics of type-2 DCPCF

In this subsection, the Raman amplification properties of type-2 DCPCF are described. The power evolution of three pumps and 24 signals along the fiber distance is depicted in Fig. 7(a). The dotted, dashed, and solid red curves correspond to pumps 1, 2, and 3, respectively, while the solid blue curves stand for the signals. The spectral variation of the gain for the individual set of pump powers is illustrated in Fig. 7(b), where, the solid red curve dictates the scenario when one pump was set to propagate, the solid black curve corresponds to two pump case, and the solid blue curve stands for three pump case. The GR for each set of pumps varies as ±0.78 dB, ±0.35 dB, and ±0.21 dB, respectively. A peak gain of 8.4 dB can be obtained in type-2 DCPCF when three pumps are used in the backward direction. Note that an attenuation spectrum of an ULL-PCF with a raised value of 0.58 dB/km at 1550 nm is taken into account to compute its amplification properties.

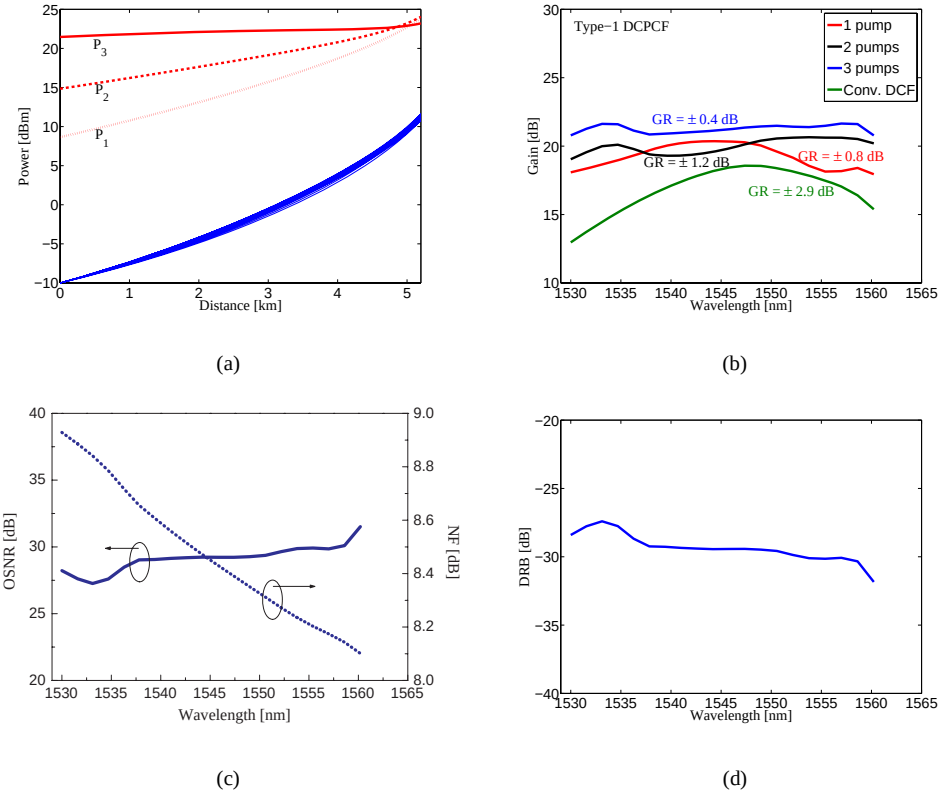

Fig. 6. (a). Power evolutions of pumps and signals along the distance of the fiber, the spectral variation of (b). gain, (c). OSNR and NF, and (d). DRB in a 5.2 km long type-1 DCPCF Raman amplifier. It can be clearly seen that with three pumps, the fiber shows GR of ±0.4 dB with a maximum gain of 21.6 dB at the expense of 690 mW of total pump power over C-band.

Table 3. Optimized pump profile for a 5.2 km long type-1 DCPCF Raman amplifier module.

m	λ_1 [nm]	λ_2 [nm]	λ_3 [nm]	P_1 [mW]	P_2 [mW]	P_3 [mW]	Total power [mW]	GR [dB]	Max gain [dB]	OSNR ripple [dB]
1	1450.0			520			520	±1.2	20.4	±2.8
2	1427.0	1458.5		360	410		770	±0.8	20.6	±1.0
3	1426.6	1448.6	1460.3	240	250	200	690	±0.4	21.6	±2.1

#78520 - $15.00 USD Received 2 January 2007; revised 31 January 2007; accepted 20 February 2007

Table 4. Optimized pump profile for a 2.73 km long type-2 DCPCF Raman amplifier module.

m	λ_1 [nm]	λ_2 [nm]	λ_3 [nm]	P_1 [mW]	P_2 [mW]	P_3 [mW]	Total power [mW]	GR [dB]	Max gain [dB]	OSNR ripple [dB]
1	1463.4			890			890	±0.78	9.2	±0.63
2	1427.9	1468.4		480	630		1100	±0.35	8.6	±0.63
3	1427	1456.7	1470.6	490	180	460	1140	±0.21	8.4	±0.64

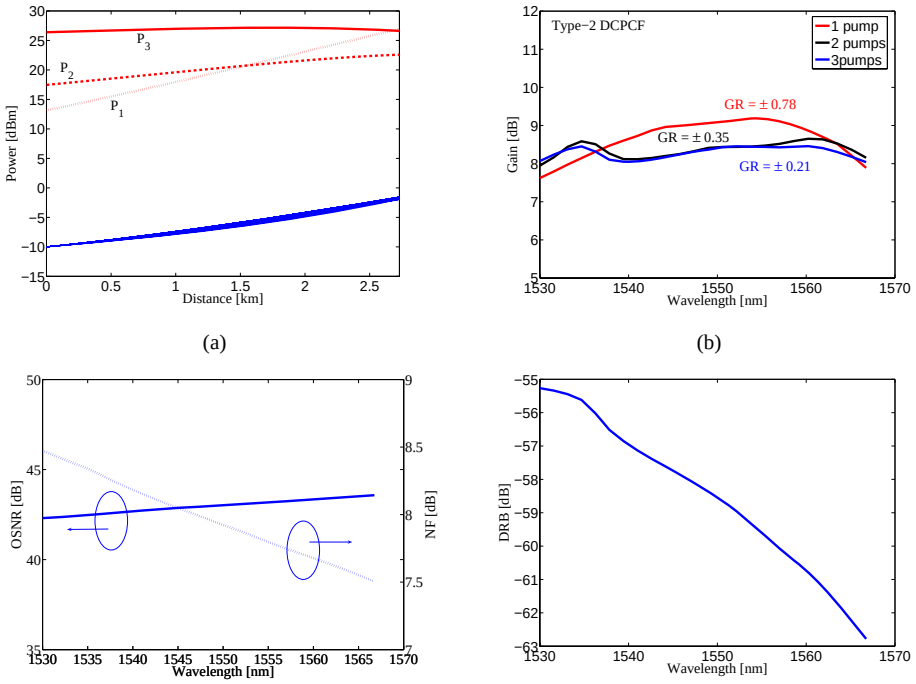

Fig. 7. (a). Power evolutions of pumps and signals along the length of the fiber, the spectral variation of (b) gain, (c) OSNR and NF, and (d) DRB in a 2.73 km long optimized type-2 DCPCF Raman amplifier. It can be clearly seen that with three pumps, the fiber shows GR of ±0.21 dB with a maximum gain of 8.4 dB at the expense of 1.1 W of total pump power over C-band.

The spectral variation of OSNR and NF is shown in Fig. 7(c) while DRB variation is exhibited in Fig. 7(d). It is revealed from the noise performances of the fiber that it supports high OSNR (> 43 dB) with ±0.6 dB ripples, low NF (<8 dB), and low DRB (<–58 dB). This ensures better performance of type-2 DCPCF in comparison to OFS-Laboratory's DCF Raman amplifier [35] whose typical characteristics are; DRB<–48 dB, NF<9 dB, GR < ±0.38 dB, and effective area of 18.7±1.5 μm^2. The pump spectrum for individual set of pumps is tabulated in Table 4, where the index *m* presents the number of pumps.

Next, we have compared the Raman gain for different attenuation levels. Due to complex geometry of fibers, they may exhibit larger attenuation coefficients than the assumed attenuation value of 0.58 dB/km at 1550 nm. To compute the impact of background losses on the gain characteristic, we have considered attenuation spectrum of ULL-PCF which was normalized and then raised to a level of a 5 dB/km at 1550 nm keeping a constant spectral

#78520 - $15.00 USD Received 2 January 2007; revised 31 January 2007; accepted 20 February 2007

variation. We expect that with the present fabrication technology the fiber may show this loss value, however, with progress in the development of fabrication procedure/technique, losses in such PCF designs can be lowered to the level of conventional DCFs. Figure 8 represents the spectral variation of gain attained in type-2 DCPCF Raman amplifier module for two different attenuation levels. It can be interpreted from the figure that the gain decreases (solid red curve) as the attenuation increases, which is as expected. We would like to mention that in a real situation, the attenuation spectral variation of DCPCF may change from the considered spectrum, thus may scale the gain values as well as the GR.

Through a comparative study between type-1 and type-2 DCPCF Raman amplifier, it has been examined that type-1 DCPCF has higher Raman gain than type-2 DCPCF, which is due to higher RGE and longer length of type-1 DCPCF in comparison to type-2 DCPCF.

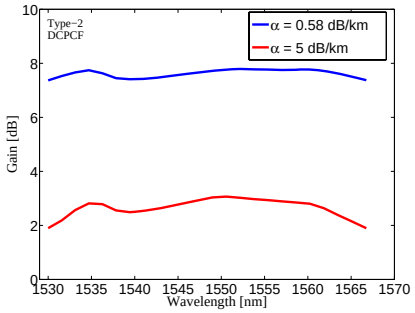

Fig. 8. Gain variation of type-2 DCPCF Raman amplifier module for two different attenuation levels. Solid blue and red curves stand for the loss levels of 0.58 dB/km and 5 dB/km at 1550 nm.

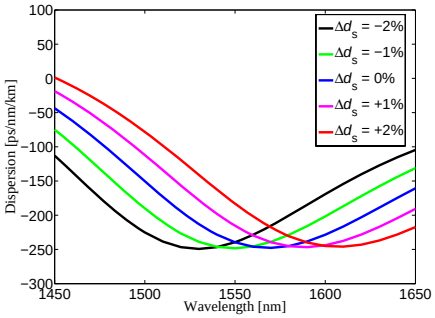

Fig. 9. Dispersion characteristics as a function of the wavelength for type-1 DCPCF for different tolerance values in d_s.

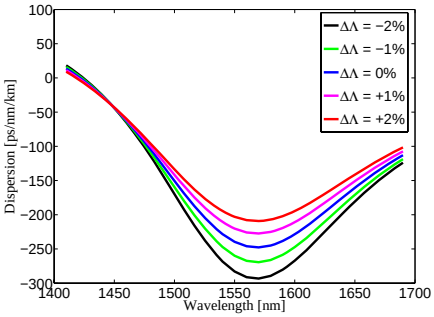

Fig. 10. Dispersion characteristics as a function of the wavelength for type-1 DCPCF for different tolerance values in Λ.

5. Tolerance study and feasibility aspects

To meet the fabrication requirements and mass production of the proposed DCPCF designs, we have extensively carried out structural tolerance analysis for different fiber design parameters; pitch constant Λ, ring-hole size d_s, and air-hole size d, which determine the device performances. To know the impact of structural deformations on the module performances, we vary one parameter, for example d_s, and fix other parameters such as Λ and d. Figure 9 depicts the dispersion characteristics of type-1 DCPCF for the change in ring's hole diameter d_s which is varied within ±2% tolerances from its nominal value. It can be evident from the figure that the minimum of the dispersion curve shifts toward left when d_s is decreased to –1% (solid green curve) and –2% (solid black curve), while the dispersion shifts toward right for

#78520 - $15.00 USD Received 2 January 2007; revised 31 January 2007; accepted 20 February 2007

+1% (solid magenta curve) and +2% (solid red curve) variation in d_s. This shift in dispersion curves results due to the shift of the PMW. The decrement in d_s may result into weak overlap of the pump and signal fields which may further decrease the gain efficiency, while the increment in d_s may lead to a strong overlap of the pump and the signal fields thus enhancing the RGE.

Figure 10 shows the tolerances in the pitch constant of the fiber. It can be concluded from the graph that for –1% (solid green curve) and –2% (solid black curve) change in the pitch constant Λ, the absolute magnitude of dispersion coefficient increases while it decreases for +1% (solid magenta curve) and +2% (solid red curve) variation, which is contrary to the effect observed in hole diameter *d* tolerances. It is noticed that a ±2% tolerance in pitch may change the absolute magnitude of dispersion coefficient by a ±16% and may also vary the RGE by a ±8%, while the RGE remains almost insensitive (<0.9%) to deformations in hole diameter *d*.

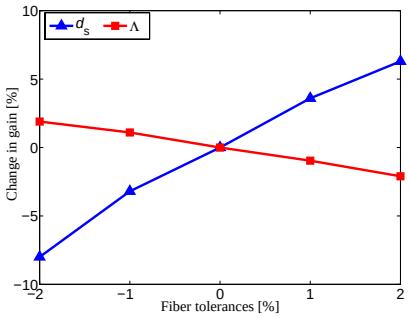

Fig. 11. Impact of fiber tolerances on the gain of type-1 DCPCF for structural variation in d_s (filled blue triangles) and pitch (filled red squares).

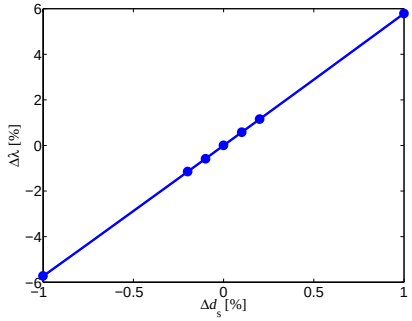

Fig. 12. Shift of PMW as a function of tolerance in d_s in type-2 DCPCF. It is evident that ±1% change in d_s may shift the PMW by ±6%.

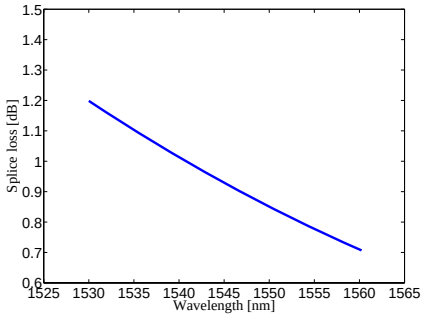

Fig. 13. Spectral variation of splice loss between type-1 DCPCF and conventional SMF in absence of any misalignments.

Next, we evaluate the impact of structural deformations of d_s and Λ on the Raman gain performances of type-1 DCPCF module. We have considered a maximum of ±2% tolerances that may occur during the fabrication of the proposed fiber design. Figure 11 illustrates the percentage change in the Raman gain that may take place by the presence of possible tolerances in Λ and d_s. The blue color filled triangles stand for the tolerances in d_s, while the red color filled squares correspond to the tolerances in Λ. It can be clearly observed from the curves that a ±2% change in d_s may lead to a ±7% change in the gain values of type-1 DCPCF Raman amplifier module, while a ±2% variation in the pitch constant Λ may modify the gain

#78520 - $15.00 USD Received 2 January 2007; revised 31 January 2007; accepted 20 February 2007

performances by a ±2%. It adds evidence from this tolerance analysis that Raman performances of the fiber are more sensitive to the deformations in d_s.

Further, we perform the sensitivity analysis for type-2 DCPCF where the ring core is built by 2nd-7th air hole rings. Here, we have evaluated the impact of hole-diameter d_s of the ring's core on the dispersion characteristics after confirming from previous analysis that d_s is more sensitive to structural deformations. We observed that a ±1% change in d_s shifts the minimum of the dispersion curves to right or left hand side. The wavelength corresponding to the minima of each dispersion curves has been noted and the shift in the corresponding wavelength (represented by $\Delta\lambda$) for minima of each dispersion curves is evaluated and plotted in Fig. 12 as a function of the change in d_s. It can be seen from the figure that −1% decrease in d_s may shift the PMW by a −6%, and hence may decrease the gain efficiency of type-2 DCPCF Raman amplifier module and thus overall Raman gain.

Finally, we calculate the splice loss between type-1 DCPCF module and a conventional SMF based on standard mode-field diameter definition and assuming absence of misalignments between the spliced fibers. The splice loss decreases linearly with the increment in wavelength (see Fig. 13). An average splice loss of 0.94 dB is obtained with a splice loss value of 0.84 dB at 1550 nm. However, the splice loss between conventional fiber and DCPCFs can be further reduced by splicing the fibers by the methodology presented in Ref. [36] that is by adopting buffer/ferrule technique [36], the splice loss can be reduced below 0.6 dB. Another important concern about type-1 and type-2 DCPCFs is the fabrication. The geometrical parameters of both DCPCFs allow the fabrication of them as a similar DCPCF with dual concentric core and smallest pitch of 1 μm was successfully fabricated by Roberts *et al*. [37]. We believe that by using the same fabrication methodology, the proposed DCPCF designs can be fabricated within allowable tolerances.

6. Summary

To summarize our work, we have optimized the pump spectra to achieve flat-Raman gain characteristics for different kind of PCFs by employing a GA optimization technique. The design parameters for type-2 DCPCF have been optimized by combining GA to V-FEM. In the optimization of pump spectra (i.e. pump power and wavelength), three pumps in the backward direction were fixed for numerical simulations as our main aim was to lower the GR by utilizing the less number of pumps. However, the optimization procedure can be extended even for larger number of pumps and can also be applied to bi-directional pump schemes, which can be useful to have effective control of NF as well as gain and such study is currently under investigation. The ULL-PCF, type-1, and type-2 DCPCFs show the lowest GR of ±0.36 dB, ±0.4 dB, and ±0.21 dB, with peak gain values of 8.8 dB, 21.4 dB, and 8.4 dB, respectively, when three backward pumps are used. We have also carried out an extensive tolerance analysis to show the performances of the device under practical situation. It can be extracted from the sensitivity analysis that the Raman performances as well as the dispersion characteristics are more sensitive to the structural deformations in the hole-diameter d_s of the air-holes in the ring core. A ±2% variation in d_s may lead to a ±7% change in the Raman gain and may shift the absolute magnitude of the dispersion coefficient by a ±16 %.

Through numerical simulations, it was observed that PCFs can serve as a suitable Raman gain medium to provide amplification with integrated dispersion compensation functionality. However, there is an experimental gap towards the realization of such PCF designs. We hope to stir the experimentalist to come forward for the fabrication of dispersion compensating PCF structures with added Raman amplification properties, as PCFs can be appropriate platforms to compensate for the dispersion in transmission networks.

Acknowledgments

Authors acknowledge to 21st Century COE (Center of Excellence) program: Meme-Media Technology Approach to the R&D of the Next Generation Information Technologies and

Indo-Japan collaboration project on: Infrastructural Technology for Advanced Use of Photonic Crystal Fibers in Optical Communication Systems.

#78520 - $15.00 USD Received 2 January 2007; revised 31 January 2007; accepted 20 February 2007